LAWRENCE
LIVERMORE
NATIONAL
LABORATORY

UCRL-JRNL-225792

Impedance Characterization of a Model Au/Yttria-Stabilized Zirconia (YSZ)/Au Electrochemical Cell in Varying Oxygen and NOx Concentrations

L. Y. Woo, L. P. Martin, R. S. Glass, R. J. Gorte

November 2, 2006

Journal of the Electrochemical Society

Disclaimer

Impedance Characterization of a Model Au/Yttria-Stabilized Zirconia (YSZ)/Au Electrochemical Cell in Varying Oxygen and NO_x Concentrations

Leta Y. Woo[a], L. Peter Martin[b], Robert S. Glass[a], and Raymond J. Gorte[c]

[a] *Energy and Environment Directorate and* [b] *Mechanical Engineering Directorate, Lawrence Livermore National Laboratory, Livermore, California 94551, USA*

[c] *Department of Chemical and Biomolecular Engineering, University of Pennsylvania, Philadelphia, Pennsylvania 19104, USA*

Abstract

An electrochemical cell (Au/YSZ/Au) serves as a model system to investigate the effect of O_2 and NO_x. Possible mechanisms responsible for the response are presented. Two dense Au electrodes are co-located on the same side of a dense YSZ electrolyte and are separated from the electrolyte by a porous YSZ layer, present only under the electrodes. While not completely understood, the porous layer appears to result in enhanced NO_x response. Impedance data were obtained over a range of frequencies (0.1 Hz to 1 MHz), temperatures (600 to 700°C), and oxygen (2 to 18.9%) and NO_x (10 to 100 ppm) concentrations. Spectra were fit with an equivalent circuit, and values of the circuit elements were evaluated. In the absence of NO_x, the effect of O_2 on the low-frequency arc resistance could be described by a power law, and the temperature dependence by a single apparent activation energy at all O_2 concentrations. When both O_2 and NO_x were present, however, the power-law exponent varied as a function of both temperature and concentration, and the apparent activation energy also showed dual dependence. Adsorption mechanisms are discussed as possibilities for the rate-limiting steps. Implications for impedancemetric NO_x sensing are also discussed.

Introduction

The development of NO_x sensors has been motivated primarily by environmental concerns and the automotive industry's desire to monitor gases in the exhaust stream.[1] Fast, reliable sensors are needed in order to meet increasingly stringent governmental regulations for emission limits. Ceramic metal oxides are candidate materials for operation in harsh, high-temperature environments, especially the oxygen-ion conductor yttria-stabilized zirconia (YSZ). YSZ is currently used for automotive oxygen sensors and has shown good stability and operation at temperatures 700°C and higher.[1–3]

NO_x sensor development poses significant challenges due to a number of issues including cost, sensitivity, stability, and response time. In the past decade, development of YSZ-based NO_x sensors has focused on amperometric and potentiometric operation.[1–3] Amperometric operation typically measures a diffusion-limited current and has been shown to be effective as an NO-selective or a total-NO_x sensor. Typically, research focuses on various metal-oxide electrodes to optimize the response.[4–7] In order to isolate the NO_x from the O_2 response, a separate pumping cell may be necessary to maintain a constant O_2 concentration at the sensing electrode, leading to complicated device structures.[1–3] Potentiometric sensors correlate the measured open circuit potential (OCP) to the gas composition. The OCP can be measured between an electrode in the test atmosphere and another electrode in reference gas, or between dissimilar electrodes in the same atmosphere. In

potentiometric operation, the response to NO_2 is generally opposite in sign to that of NO, and generally larger, making total-NO_x sensing difficult.[8]

More recently, a YSZ-based impedancemetric technique has been reported for sensing of NO_x and CO.[9–12] In that technique, the modulus (or magnitude) of the measured complex impedance at $\leq$1 Hz serves as the sensing signal. NO and NO_2 were shown to produce similar responses, offering the potential for total-NO_x sensing. Impedancemetric NO_x sensors show promise for overcoming the problems associated with amperometric (complex device structures) and potentiometric (interference between NO and NO_2) sensors; however, a better understanding of the sensing mechanisms is necessary to optimize sensor operation.

Previous work has demonstrated the effectiveness of an impedancemetric NO_x sensor using dense Au, porous YSZ/Cr_2O_3 composite electrodes, and a YSZ electrolyte in an in-plane geometry (i.e., both electrodes are co-located on the same side of the electrolyte).[12] In an effort to better understand the sensing mechanism, the present work uses a model electrochemical cell to isolate the role of the Au/porous YSZ interface. Using an in-plane geometry, the model system consists of a dense YSZ electrolyte and two planar Au plates, with a porous YSZ layer separating the Au and dense YSZ. Electrochemical characterization of the model cell involves impedance measurements that are then fit with an equivalent circuit. Data taken at different temperatures and concentrations are used to interpret the effect of O_2 and

NO_x.

Understanding the cross-sensitivity to interfering gases (e.g., water vapor, hydrocarbons, etc.) is also crucial for sensor operation, but a comprehensive study is outside the scope of the current work. For automotive exhaust applications, interference from hydrocarbons and other gases may be mitigated using separate strategies. A cross-sensitivity study in conjunction with automotive dynamometer testing of a prototype impedancemetric YSZ-based sensor is being conducted and will be the subject of a separate study. The present analysis provides a base from which future work on the role of different oxides (e.g., Cr_2O_3), microstructures (e.g., porosity), and other material parameters can be examined.

Experimental

Yttria-stabilized zirconia (YSZ) powder (Tosoh 8-YS) was pressed in a uniaxial die and then sintered at 1450°C for 2 hours. The sintered pellet had a diameter of 12.2 mm with a nominal thickness of ∼1.5 mm. Porous YSZ was then spray coated onto the surface of the pellet using YSZ powder dispersed in a 50% H_2O/50% ethanol solution. The porous YSZ was deposited as two side-by-side rectangles (each with area ∼28 mm^2) with ∼0.5 mm separation, and was then fired at 1000°C for one hour. The thickness of the porous YSZ layer was ∼10 μm, as seen in the SEM image in Fig. 1a. The SEM image in Fig. 1b shows an interconnected network of ∼100 nm diameter YSZ par-

ticles. Two thin Au plates were contacted to the porous YSZ layers using constant spring-loaded pressure.

Testing was performed in a quartz tube (I.D. of 16.8 mm) placed inside a tube furnace with both electrodes exposed to the same gas flow. The gas flow rate was maintained at 500 ml/min with composition controlled by mixing air, N_2, and 1000 ppm NO or NO_2 using a standard gas handling system equipped with thermal mass flow controllers. Electrochemical measurements were performed using a Solartron Analytical SI 1260 Impedance/gain-phase analyzer with the Solartron Analytical SI 1287 electrochemical interface. Computer-controlled data acquisition used the commercially available ZPlot software (Scribner Associates, Inc.). Impedance spectra were collected by scanning the frequency from 1 MHz to 0.1 Hz at 20 steps per decade with an excitation voltage of 50 mV. Impedance spectra were analyzed using Boukamp's EQUIVCRT.COM software.[13]

Results and Discussion

Impedance Spectroscopy

The impedance of a material (Z) describes the response to an alternating signal, and includes both magnitude ($|Z|$) and phase angle (θ) information. The following relationships describe the complex impedance ($Z(\omega) = \mathrm{Re}(Z) + j\mathrm{Im}(Z)$), where $\mathrm{Re}(Z)$ is the real component and $\mathrm{Im}(Z)$ is the

imaginary component:[14]

$$\mathrm{Re}(Z) = |Z|\cos\theta \quad \text{and} \quad \mathrm{Im}(Z) = |Z|\sin\theta \tag{1}$$

The relationship for phase angle is described by the following:

$$\theta = \tan^{-1}\left(\frac{\mathrm{Im}(Z)}{\mathrm{Re}(Z)}\right) \tag{2}$$

and for the magnitude:

$$|Z| = \sqrt{(\mathrm{Re}(Z))^2 + (\mathrm{Im}(Z))^2} \tag{3}$$

For impedancemetric sensor operation, either of the measured quantities (i.e., magnitude or phase angle) at a specified frequency can serve as the sensing signal.[9–12] Impedance spectroscopy entails using a frequency response analyzer to measure the response to (typically) small amplitude excitation over a range of frequencies (spectrum). The data can be presented in a so-called Nyquist plot, which is a complex plane representation ($-\mathrm{Im}(Z)$ vs. $\mathrm{Re}(Z)$) that provides indirect information about both magnitude ($|Z|$) and phase angle (θ) over a range of frequencies. Alternatively, the data can be presented as a Bode plot, where either $|Z|$ or θ is plotted vs. log frequency.

Figure 2 shows a Nyquist plot of the Au/YSZ/Au cell at 600°C in 2% O_2 and in 2% O_2 with 100 ppm of NO. Material behavior with both resistive and capacitive components produces characteristic arcs that appear in different frequency ranges in the Nyquist representation. In Fig. 2, a discernable high-frequency arc is shown in the inset, while a larger low-frequency arc

dominates the spectra. $|Z|$ and θ at 10 Hz are graphically illustrated as solid and dotted lines, respectively, where $|Z|_1$ and θ_1 refer to the response in 2% O_2, and $|Z|_2$ and θ_2 refer to the response in 2% O_2 with 100 ppm of NO. The cell behavior at higher frequencies, above $\sim 10^3$ Hz, does not change with NO (see inset of Fig. 2). However, the diameter of the large arc at lower frequencies decreases significantly with the introduction of NO. Corresponding decreases can be seen in both the magnitude (from $|Z|_1$ to $|Z|_2$) and phase angle (from θ_1 to θ_2) at 10 Hz. The response to NO_2 was qualitatively similar to that for NO, but slightly smaller under certain conditions. These differences are further discussed below.

Miura et al.[10] and Wu et al.[11] have seen qualitatively similar impedance response using $ZnCr_2O_4$ and Au-Ga_2O_3 sensing electrodes to detect NO_x and CO, respectively. In Ref. 10, the counter electrode was Pt exposed to atmospheric air, with only the $ZnCr_2O_4$ sensing electrode exposed to the test atmosphere. In Ref. 11, the Au-Ga_2O_3 sensing electrode and Pt reference electrode were both exposed to the same test atmosphere. Sensors using different electrodes and atmospheres may induce corresponding voltage changes (open circuit potentials) due to different reactions or kinetics at the electrodes, an effect usually explained with "mixed potential" or "differential electrode equilibria" theory. The mixed potential theory refers to differences in equilibria between electrochemical NO_2/NO and O_2 reactions taking place at the electrodes.[8,9,15] Differential electrode equilibria

theory is a more general term that includes non-equilibrium phenomena and changes in chemical adsorption behavior of the electrodes.[16,17] The measured impedance, however, only reflects the material phenomena, and not the induced EMF, as long as small-amplitude fields are applied to prevent the possibility of microstructural damage. In the current work, both electrodes of the model cell are identical and exposed to the same test atmosphere.

Miura et al. and Wu et al. utilized the magnitude (or modulus) $|Z|$ as the sensing signal at low frequencies, 1 Hz and 0.42 Hz, respectively.[10,11] In the current work, the phase angle (θ) response is also investigated for use as a sensing signal.[12] Figure 3a shows Bode plots demonstrating the variation of $|Z|$ and θ with frequency for the model cell at 600°C in 2% O_2 and 2% O_2 with 100 ppm of NO. Figure 3a demonstrates that the θ response persists to higher frequencies than the $|Z|$ response. Neither parameter exhibits any significant difference in response in the presence of NO at frequencies $\geq$1 kHz. As a measure of the sensitivity, Fig. 3b shows the fractional change in $|Z|$ and θ with the addition of 100 ppm NO. As reported in Refs. 10 and 11, the $|Z|$ sensitivity decreases with increasing frequency. However, it can be seen that the θ sensitivity passes through a weak maximum at $\sim$2 Hz. A maximum is always present since θ goes to zero as the frequency goes to zero and infinity. Furthermore, in Fig. 3b, it is shown that θ is a more sensitive indicator of NO than $|Z|$ for frequencies greater than $\sim$3 Hz. Higher frequency operation is desirable since it allows for re-

duced sampling times and potentially lower noise background.[12] Therefore, in terms of sensor operation, operating frequency may be selected as a compromise between sensitivity (lower frequencies) and reduced sampling time (higher frequencies). An analysis of the performance of a working sensor at 10 Hz is the subject of another publication.[12] The present work focuses on interpreting the response of the model electrochemical cell in the range of ~10 Hz to varying O_2 and NO_x concentrations.

Equivalent circuit analysis

The Nyquist representation of impedance spectra for material phenomena exhibiting both resistive and capacitive components (e.g., grain boundaries, interfaces, etc.) often produces the characteristic semicircular arcs seen in Fig. 2. The discrete arcs represent processes with distinguishably separate characteristic time constants (τ). For a perfect resistor and capacitor in parallel, the diameter of the arc corresponds to the magnitude of the resistance (R). The angular frequency at the top of the arc (ω_{top}) is related to the value of the capacitor (C) through the time constant τ ($\tau = R \times C$) using the following relationship:

$$\omega_{top} = \frac{1}{\tau} = \frac{1}{RC} \tag{4}$$

At least two orders of magnitude difference between time constants are necessary to produce clearly separated arcs. Unfortunately, in real material systems, it is often the case that multiple phenomena have similar time con-

stants (less than two orders of magnitude difference). This causes the arcs to be overlapped and convoluted. In addition, for real non-ideal systems, heterogeneity in the behavior, especially at interfaces, may lead to distributions of time constants. This typically causes "depressed" arcs, where the center of the arc lies below the real axis of the Nyquist plot. One way to simulate the non-ideal behavior is to replace the capacitor with a constant phase element (CPE) in the equivalent circuit. The CPE has the following impedance relationship:[14]

$$Z(\omega) = \frac{1}{Y_0(j\omega)^{-n}} \tag{5}$$

where Y_0 is a constant, ω is angular frequency, and n is a measure of arc-depression:

$$n = 1 - \frac{2\phi}{\pi} \tag{6}$$

The angle of the arc depression below the real axis of the Nyquist plot is given by ϕ. For $n = 0$, the impedance reduces to a resistor with a value of Y_0^{-1}, and for $n = 1$, the impedance reduces to a capacitor with a value of Y_0. For values of n approaching 1, it is common practice to use the Y_0 value as an approximation for capacitance.

It should be noted that interpretation of the Nyquist plot is not always straightforward. For instance, while changes in resistive behavior are clearly evidenced by decreasing arc diameters, for example with the addition of NO_x, changes in capacitive behavior are not as easily quantified. For this reason, equivalent circuit analysis is commonly used to quantify the

response of electrochemical cells in terms of various circuit elements (i.e., resistors, capacitors, inductors, etc.). In the present work using the model electrochemical cell, the addition of NO_x induces changes primarily in the low-frequency behavior, which can be approximated with a single arc and is considered separately from the remaining higher frequency response.

Figure 4 shows the equivalent circuit used to fit the low-frequency arc where a resistor (R_S) is in series with a subcircuit that consists of a resistor (R_{LF}) in parallel with a constant phase element (CPE). The subscripts "S" and "LF" stand for series and low-frequency, respectively. Note that the value of R_S approximates the high-frequency contribution to the total cell resistance. The value of R_{LF} corresponds to the diameter of the low-frequency arc, where the CPE (defined by Y_0 and n, see Eq. 5) is related to the frequency at the top of the low-frequency arc and the amount of arc depression. The experimental impedance data were fit by using the partial non-linear least squares fitting routine in the Boukamp EQUIVCRT.COM software.[13] The n-values derived from the fitting procedure vary from $\sim$0.88 to $\sim$0.90 and show no temperature or concentration dependence. Since these values of n approach one, the best-fit values of Y_0 in the CPE are used to approximate capacitance. Typical results from the fitting procedure using the equivalent circuit are shown as solid lines in Fig. 5 and are discussed in detail below.

Modeled behavior: Low-frequency arc

Figure 5 shows typical behavior of the model electrochemical cell at 600°C in 2% O_2 and with 10, 50, and 100 ppm additions of NO. Discrete points represent the experimentally measured data, and the solid lines are the best-fit using the equivalent circuit in Fig. 4. Although the behavior predicted by the equivalent circuit deviates from the experimental data in the frequency extremes <1 Hz and >1 kHz (as seen in Fig. 5), there is excellent agreement over most of the frequency range. More importantly, the equivalent circuit accurately describes the behavior of the model electrochemical cell in the frequency range around 10 Hz, which is the desired frequency range for sensor operation.[12]

Figure 5 also shows the impedance behavior of the model electrochemical cell with the addition 8.5% O_2 (for a total of 10.5% O_2), as represented by the shaded squares. The Nyquist behavior shows comparable decreases in the low-frequency arc diameters when either 8.5% O_2 or 100 ppm NO (open circles) is introduced. This corresponds to decreases in R_{LF} of ∼64% with the addition of 8.5% O_2 and ∼52% with the addition of 100 ppm NO. Therefore, the impedance response to O_2 and NO_x are similar when the NO_x concentration is about three orders of magnitude smaller than the O_2 concentration (i.e., 8.5%=85,000ppm). The implication is that although both O_2 and NO_x reduce the low-frequency arc diameter (R_{LF}), NO_x causes significantly more pronounced changes in the electrical response.

To develop a better understanding of the effects of O_2 and NO_x with the model electrochemical cell, the impedance behavior is interpreted using the equivalent circuit to evaluate possible rate-limiting mechanisms. The approach involves comparing the calculated values of the circuit elements (i.e., the best-fit of the equivalent circuit to the experimentally measured data) as a function of both gas concentration and temperature. Analysis of the effect of O_2 is presented first, followed by the anlaysis of the behavior when NO_x is introduced.

Oxygen behavior

The effect of oxygen partial pressure, P_{O_2}, on the values of the resistances (R_S and R_{LF}) is shown in Fig. 6a. R_S is insensitive to P_{O_2} and is likely dominated by the ohmic contributions from the leads and contacts and the ionic contribution from the dense YSZ electrolyte. R_{LF} shows identical P_{O_2} dependences at all temperatures, with $R_{LF} \propto P_{O_2}^{-0.62}$. A P_{O_2} dependence of $R_{LF} \propto P_{O_2}^{-0.5}$ has been suggested when dissociative adsorption of oxygen is the rate-limiting step.[18–20] It is also possible that a surface diffusion process could produce a similar dependence on P_{O_2}; however, in that case diffusion-limited current behavior would be expected, and that was not observed in the present cell. The deviation of the measured power-law exponent (-0.62) from -0.5 could result from some additional contribution from processes other than dissociative adsorption. Possibilities include gas-phase diffusion or molecular adsorption, both of which produce a power-law exponent of

-1.[18] Therefore, dissociative adsorption probably dominates the response with some contribution from other processes.

Investigation of the temperature dependence yielded an apparent activation energy for R_{LF} of 98 kJ/mol for all O_2 concentrations, as shown in Fig. 6b. Since R_S does not show any P_{O_2} dependence, the average values at all O_2 concentrations investigated (2 to 18.9%) are shown and used to calculate an apparent activation energy of 93 kJ/mol. This activation energy for R_S is consistent with ionic diffusion in the dense YSZ. The similarity between the apparent activation energies of R_S and R_{LF} may indicate that a diffusion mechanism is also responsible for R_{LF}; however, no diffusion-limited current behavior was observed. The discrepancy could indicate a complex rate-limiting mechanism involving both diffusion and adsorption or similar activation energies for diffusion and adsorption.

Alternatively, an apparent activation energy of 89 kJ/mole has been reported for the electrode behavior of an Au, O_2(g)/YSZ system.[21] In another study, Hertz et al. found that the electrode behavior of lithographically patterned electrodes on thin film YSZ electrolytes depends on the electrode material, exhibiting activation energies of 0.91 eV (88 kJ/mol) for gold electrodes and 0.77 eV (74 kJ/mol) for platinum electrodes.[22] The similarity between these reported values and the measured apparent activation energies in the present work may indicate that the mechanism(s) responsible for the oxygen response are related to the Au/YSZ interface.

The P_{O_2} dependence of the capacitance calculated from the equivalent circuit is shown in Fig. 6c. Recall that for values of n approaching one, the best-fit values of Y_0 in the CPE approximate capacitance. As seen in Fig. 6c, the calculated capacitances exhibit only slight dependence on temperature or P_{O_2}, in all cases within the range of 0.32 to 0.37 μF. However, general trends in the data indicate that capacitance increases with P_{O_2}. For example, the capacitance increases similarly with P_{O_2} at 600 and 650°C, ∼9%, when P_{O_2} increases from 2 to 10.5%, and ∼14% when P_{O_2} increases from 2 to 18.9%. This increase in capacitance with P_{O_2} may be related to an increase in the fraction of adsorbed O_2 species at the Au/YSZ interface.[21,23] At 700°C, the capacitance increases only ∼2% when P_{O_2} increases from 2 to 10.5% and ∼4% when P_{O_2} increases from 2 to 18.9%. The amount of capacitance change at 700°C is not significant. Since the measured capacitance changes are small, care should be taken in making concrete conclusions. Nevertheless, the trends, especially at lower temperatures, indicate that adsorbed O_2 species at the Au/YSZ interface may be important in determining the measured capacitance values.

NO_x behavior

The response of the electrochemical cell to either NO or NO_2 is similar under all test conditions. The symmetric electrode configuration with both electrodes exposed to the same atmosphere seems a likely explanation for the similar response to NO and NO_2. The similar response may also be due

to thermodynamic equilibration of the NO/NO_2 ratio, which will result in identical gas compositions regardless of whether NO or NO_2 is introduced initially. NO is more stable than NO_2 at temperatures >600°C, and thermodynamic calculations predict ∼90% NO, balance NO_2.[24] However, the calculated values of R_{LF} are slightly larger with the addition of NO_2 relative to NO, ranging from ∼0.1% to ∼11%. Experimental error associated with the accuracy of the mass flow controller may account for some of the difference, but there are consistent trends with temperature and composition. General trends include larger differences between NO and NO_2 with increasing concentration and at lower temperature.

Yoo et al. performed temperature-programmed reaction (TPR) experiments using NO/NO_2 and O_2 gas mixtures as the reactant gas over a YSZ-8Y substrate. They demonstrated that only gas-phase NO_2 decomposition occurs:[24]

$$NO_2 \leftrightarrow NO + \frac{1}{2}O_2 \tag{7}$$

Yoo et al. also showed that when NO_2 is introduced, the reaction remains incomplete at temperatures <700°C without an appropriate catalyst, and leads to non-equilibrium gas compositions.[24] The addition of NO causes little change in overall gas composition since only ∼10% reacts to form NO_2, and the kinetics have been shown to be relatively fast.[24] In the present study, the minimal catalytic ability of the Au/YSZ system probably does not allow complete equilibrium decomposition of NO_2, especially at the lower

temperatures. Larger amounts of NO_2 would also be expected to remain unreacted for larger concentrations of NO_2. Therefore, larger deviations from the equilibrated NO/NO_2 ratio are expected at lower temperatures and larger concentrations. The deviations result in smaller amounts of NO and larger amounts of NO_2 than predicted by thermodynamic equilibrium. If adsorption is the prevailing mechanism, NO_2 may not have as many sites available for adsorption due to its relatively larger size.[8] If this were the case, the amount of NO determines the impedance response and decrease in R_{LF}. It is possible that the larger values of R_{LF} calculated for NO_2 are due to a reduction in the amount of NO from non-equilibrium conditions. This effect would then be expected to be more pronounced at lower temperatures and higher concentrations, as seen in the current study. The data collected in the current study only provide a preliminary investigation into mechanistic details leading to response differences between NO and NO_2. Further studies are required to explain the exact mechanism.

The effect of NO_x concentration on the resistances (R_S and R_{LF}) was qualitatively similar to the effect of O_2, where R_S was insensitive to NO_x concentrations. The NO_x dependence of the low-frequency resistance (R_{LF}) was determined by accounting for the effect of oxygen:

$$\frac{1}{R_{LF/NO_x}} = \frac{1}{R_{LF/O_2+NO_x}} - \frac{1}{R_{LF/O_2}} \tag{8}$$

where R_{LF/NO_x} is the resistance contribution for NO_x, R_{LF/O_2+NO_x} is the R_{LF} measured when both O_2 and NO_x are present, and R_{LF/O_2} is the R_{LF}

measured when only O_2 is present. In the range 10 to 100 ppm of NO_x, the $R_{LF/NO_x} \propto [NO_x]^{\alpha}$, with $\alpha = -0.96 \pm 0.04$ and $\alpha = -1.02 \pm 0.16$ for NO and NO_2, respectively, as shown in Fig. 7. R_{LF/NO_x} was effectively insensitive to temperature and P_{O_2}, so the average values are shown in Fig. 7 with error bars indicating the standard deviation.

A possible explanation for the dependence of R_{LF/NO_x} on the NO_x concentration is a rate-limiting step controlled by the molecular adsorption of NO (non-dissociative adsorption). This is analogous to the case of molecular adsorption of O_2 which, when acting as the rate-limiting step, results in a power-law exponent of -1.[18] In the current cell, dissociative adsorption of NO is not expected based on prior reports that the process requires either an appropriate catalyst (e.g., Pt, Rh, and Pd)[25] or high electric fields.[26–28] In addition, the absence of limiting current behavior suggests that gas phase diffusion is not responsible for the NO_x behavior. Thus, the NO_x dependence of R_{LF/NO_x} appears to be consistent with the non-dissociative adsorption of NO_x. Furthermore, since the calculated R_{LF/NO_x} from Eq. 8 is independent of O_2, it appears that the impedance behaviors of O_2 and NO_x have parallel contributions to the overall measured impedance. Therefore, the parallel behavior of O_2 and NO_x, which have different concentration dependences, $R_{LF} \propto P_{O_2}^{-0.62}$ and $R_{LF/NO_x} \propto [NO_x]^{-1}$, results in larger changes in impedance for NO_x compared to O_2.

In general, the temperature dependence of R_{LF/NO_x} results in negative

apparent activation energies, which indicates an increase in R_{LF/NO_x} with temperature. This is in contrast to the response of the cell in the absence of NO_x, where R_{LF} decreases with temperature (see Fig. 6b). Increasing resistance with temperature has been attributed to adsorption processes, where the magnitude of the apparent activation energy is related to the surface coverage.[29,30] The magnitudes of the apparent activation energies for NO range from 0.3 to 6 kJ/mol for varying relative concentrations of NO (10 to 100 ppm) and O_2 (2 to 18.9%), indicating little temperature sensitivity. The exception is a mixture of 18.9% O_2 (high oxygen) and 10 ppm NO gas mixture, which produces a slightly larger magnitude of 12 kJ/mol for the apparent activation energy. The magnitude of the apparent activation energies in O_2 mixtures for NO_2 are larger than those for NO. For 50 and 100 ppm NO_2, apparent activation energies range from 1 to 14 kJ/mol. For 10 ppm NO_2, apparent activation energies range from from 37 to 54 kJ/mol. In general, the magnitude of the apparent activation energy appears to decrease as NO_x concentration increases and O_2 concentration decreases. However, there is considerable scatter in the data. If surface coverage is the dominant factor, the results may indicate larger surface coverage for either larger concentrations of NO_x or smaller concentrations of O_2, with NO showing more pronounced adsorption than NO_2, as discussed above. Although further studies are needed to explain the temperature dependence of R_{LF/NO_x}, the data seem to support a rate-limiting adsorption mechanism being responsi-

ble for the sensing behavior.

The capacitance values for any combination of O_2 (2, 10.5, and 18.9%) and NO_x (10, 50, and 100 ppm) concentrations and temperatures (600, 650, and 700°C) were similar, with values ranging from 0.31 to 0.39 μF. At 650 and 700°C, NO_x had no effect, within experimental error, on the measured capacitance calculated from the low-frequency arc. Larger changes in capacitance were measured at 600°C; however, the differences are <9%. The small changes in capacitance (<9%) at all temperatures do not allow any definitive mechanistic conclusions, regarding the effect of either O_2 or NO_x, be made in the concentration ranges investigated.

O_2 and NO_x interaction

The P_{O_2} dependence of the cell was calculated at each NO_x concentration and temperature. The behavior is similar to that when only oxygen is present with $R_{LF} \propto P_{O_2}^{\beta}$, but with variations in the power-law exponent depending on the NO_x concentration and temperature, as seen in Table 1. The absolute value of β decreases with additions of NO_x, an effect that becomes more pronounced at lower temperatures. The values of β range from -0.62 to -0.49, where the smallest absolute value of β occurs for 100 ppm NO at 600°C.

The overall apparent activation energy of R_{LF} when both O_2 and NO_x are present varies as a function of gas compositions. Figure 8 shows the temperature dependence for the three levels of NO concentration in 2% O_2,

where the activation energy decreases for larger amounts of NO. Quantitatively, similar results were observed for NO_2. Measured apparent activation energies for R_{LF} are higher for the larger O_2 concentrations and always decrease with the addition of NO_x. Table 2 lists the apparent activation energy values for the various O_2 and NO_x concentrations. The lowest activation energy occurs for 2% O_2 and 100 ppm NO gas composition, with a value of 64 kJ/mol.

The trends, as seen in Tables 1 and 2, result from the parallel contributions of O_2 and NO_x, each having different concentration and temperature behavior, and seem to indicate a competition between the mechanisms responsible for the O_2 and NO_x responses. The behavior also implies a greater effect from NO_x at lower temperatures. While it is not completely clear at present, the behavior may result from competition for available adsorption sites. Previous work suggests that oxygen adsorption sites on Au are related to surface impurities, and no adsorption is anticipated on Au that is free of impurities.[31] The dense Au used in this study probably contains impurities, and some oxygen adsorption on the Au may be expected. Also, due to the low surface area of the dense Au, reduced catalytic activity is anticipated. Adsorption of oxygen on YSZ has been studied by Yamawaki et al.[32] In their work, a high-temperature Kelvin probe was used to monitor the in situ oxygen chemisorption on YSZ surfaces. Singly ionized atomic oxygen species were proposed to be the dominant species with a maximum surface

coverage of ∼62% at 700°C.[32] The coverage decreases linearly with temperature to ∼20% at 600°C. If O_2 and NO_x are competing for available sites, possibly more sites are available for NO_x adsorption at lower temperatures leading to a more significant effect on the O_2 partial pressure dependence.

Since adsorption processes appear to dominate the response, the decrease in apparent activation energies with the introduction of NO_x may indicate changes in the adsorption energy and heat of adsorption. The amount of equilibrium adsorbed oxygen may affect the interaction between NO_x and the surface and leads to changes that depend on both O_2 and NO_x concentration.[33]

Conclusions

Electrochemical characterization of an Au/yttria-stabilized zirconia (YSZ)/Au cell demonstrates that increases in either O_2 or NO_x concentrations decrease the low-frequency arc diameter (R_{LF}), while high-frequency behavior remains unaffected. An equivalent circuit consisting of a resistor in series with a subcircuit containing a resistor and constant phase element in parallel was used to fit the experimental data, where the resistor in the subcircuit (R_{LF}) corresponded to behavior associated with impedancemetric NO_x sensing. Examination of the concentration and temperature dependences of R_{LF} provided mechanistic information. In the absence of NO_x, a single power-law exponent (-0.62) describes the P_{O_2} dependence (2 to 18.9%) of

R_{LF} at all temperatures (600 to 700°C). Dissociative adsorption of oxygen is suggested as a possibility for the rate-limiting step. Also, when only O_2 is present, a single apparent activation energy of 98 kJ/mol describes the temperature dependence for all concentrations, which may indicate the possible role of the Au/YSZ interface.

The dependence of R_{LF/NO_x} on NO_x concentration (10 to 100 ppm) yields a power-law exponent of -1, and the molecular adsorption of NO is proposed as the rate-limiting step. When both O_2 and NO_x are present, the resulting apparent activation energies and P_{O_2} dependence vary with gas compositions and temperature, which may indicate competition between the two species. One possible explanation could be changes in the available adsorption sites for O_2 and NO_x, which vary with temperature and gas concentrations.

If adsorption processes are primarily responsible for the cell response, surface treatments of the YSZ could help to increase sensitivity and sensor signal. Also, other contributions to the impedance response, e.g., diffusion, should be minimized. Further studies to elucidate the mechanisms are currently in progress.

Acknowledgements

This work was performed under the auspices of the U. S. Department of Energy by the University of California, Lawrence Livermore National Lab-

oratory under Contract No. W-7405-Eng-48. Support for the work at the University of Pennsylvania was provided by the U.S. Department of Energy's Hydrogen Fuel Initiative (grant DE-FG02-05ER15721). Two of the coauthors (RSM and LPM) are also supported through the DOE Office of Freedom Car and Vehicle Technologies. We gratefully acknowledge the support of the Program Manager, Rogelio Sullivan.

References

1. F. Ménil, V. Coillard, and C. Lucat, *Sens. Actuators, B*, **67**, 1 (2000).

2. W. Göpel, G. Reinhardt, and M. Rösch, *Solid State Ionics*, **136-137**, 519 (2000).

3. J. Riegel, H. Neumann, H. -M. Wiedenmann, *Solid State Ionics*, **152-153**, 783-800 (2002).

4. S. Somov, G. Reinhardt, U. Guth, and W. Göpel, *Sen. Actuators, B*, **35-36**, 409 (1996).

5. V. Coillard, H. Debéda, C. Lucat, and F. Ménil, *Sen. Actuators, B*, **78**, 113 (2001).

6. D. L. West, F. C. Montgomery, and T. R. Armstrong, *Sen. Actuators, B*, **111-112**, 84-90 (2005).

7. D. L. West, F. C. Montgomery, and T. R. Armstrong, *J. Electrochem. Soc.*, **153**, H23 (2006).

8. C. O. Park and N. Miura, *Sens. Actuators, B*, **113**, 316 (2006).

9. N. Miura, M. Nakatou, and S. Zhuiykov, *Ceram. Int.*, **30**, 1135 (2004).

10. N. Miura, M. Nakatou, and S. Zhuiykov, *Sen. Actuators, B*, **93**, 221 (2003).

11. N. Wu, Z. Chen, J. Xu, M. Chyu, and S.X. Mao, *Sens. Actuators, B*, **110**, 49 (2005).

12. L. P. Martin, L. Y. Woo, and R. S. Glass, *J. Electrochem. Soc.*, to appear.

13. B. A. Boukamp, *Equivalent Circuit (EQUIVCRT.PAS)*, University of Twente, Dept. of Chemical Engineering, The Netherlands (1990).

14. J. R. Macdonald, *Impedance Spectroscopy: Emphasizing Solid Materials and Systems*, p. 5, John Wiley & Sons, New York (1987).

15. N. Miura, G. Lu, and N. Yamazoe, *Solid State Ionics*, **136-137**, 533 (2000).

16. E. Di Bartolomeo, M. L. Grilli, and E. Traversa, *J. Electrochem. Soc.*, **151**, H133 (2004).

17. E. D. Wachsman, in *Solid-State Ionic Devices III*, E. D. Wachsman, K. Swider-Lyons, M. F. Carolan, F. H. Garzon, M. Liu, and J.R. Stetter, Editors, PV 2002-26, p. 215, The Electrochemical Society Proceedings Series, Pennington, NJ (2003).

18. Y. Takeda, R. Kanno, M. Noda, Y. Tomida, and O. Yamamoto, *J. Electrochem. Soc,*, **134**, 2656 (1987).

19. H. Fukunaga, M. Koyama, N. Takahashi, C. Wen, and K. Yamada, *Solid State Ionics*, **132**, 279 (2000).

20. M. Koyama, C. Wen, T. Masuyama, J. Otomo, H. Fukunaga, K. Yamada, K. Euguchi, and H. Takahashi, *J. Electrochem. Soc.*, **148**, A795 (2001).

21. B. A. van Hassel, B. A. Boukamp, and A. J. Burggraaf, *Solid State Ionics*, **48**, 155 (1991).

22. J. L. Hertz and H. L. Tuller, *J. Electroceramics*, 13, 663 (2004).

23. T. Kenjo and K. Wada, *Solid State Ionics*, **67**, 249 (1994).

24. J. Yoo, F. M. Van Assche, and E. D. Wachsman, *J. Electrochem. Soc.*, 153, H115 (2006).

25. D. C. Skelton, R. G. Tobin, D. K. Lambert, C. L. DiMaggio, and G. B. Fisher, *Sens. Actuators, B*, 96, 46 (2003).

26. S. Pancharatnam, R. A. Huggins, and D. M. Mason, *J. Electrochem. Soc.*, **122**, 869 (1975).

27. H. Song, J. Moon, and H. J. Hwang, *J. Eur. Ceram. Soc.*, **26**, 981 (2006).

28. T. Hibino, T. Inoue, and M. Sana, *Solid State Ionics*, **130**, 19 (2000).

29. O. J. Velle, T. Norby, and P. Kofstad, *Solid State Ionics*, **47**, 161 (1991).

30. G. Wedler, *Chemisorption: An Experimental Approach*, p. 109, Butterworths, London, England (1976).

31. N. D. S. Canning, D. Outka, and R. J. Madix, *Surf. Sci.*, **141**, 240 (1984).

32. M. Yamawaki, T. Bak, M. K. Nowotny, J. Nowotny, and C. C. Sorrell, *J. Phys. Chem. Solids*, **66**, 322 (2005).

33. M. J. Madou and S. R. Morrison, *Chemical Sensing with Solid State Devices*, p.67, Academic Press, San Diego, CA (1989).

Table 1: Power-law exponent ($R_{LF} \propto \mathrm{P}_{O_2}^{\beta}$) for various NO_x concentrations and temperatures.

	no NO_x	10 ppm NO	10 ppm NO_2	50 ppm NO	50 ppm NO_2	100 ppm NO	100 ppm NO_2
600°C	-0.63	-0.60	-0.61	-0.53	-0.55	-0.49	-0.51
650°C	-0.63	-0.62	-0.62	-0.57	-0.58	-0.54	-0.55
700°C	-0.62	-0.61	-0.62	-0.59	-0.60	-0.57	-0.58

Table 2: Apparent activation energy (kJ/mol) of R_{LF} for various O_2 and NO_x concentrations.

	no NO_x	10 ppm NO	10 ppm NO_2	50 ppm NO	50 ppm NO_2	100 ppm NO	100 ppm NO_2
2% O_2	99	92	93	76	78	64	68
10.5% O_2	98	94	94	82	84	74	76
18.9% O_2	98	95	95	85	86	77	79

List of Figures

of R_S and R_{LF}, and (c) the P_{O_2} dependence of capacitance at different temperatures (see text for details).

Fig. 7: NO_x concentration dependence of R_{LF/NO_x} (see text) for (a) NO and (b) NO_2. Since R_{LF/NO_x} was insensitive to temperature and P_{O_2}, average values are shown with error bars indicating the standard deviation.

Fig. 8: Temperature dependence of the low-frequency resistance, R_{LF}, for 10, 50, and 100 ppm NO in 2% O_2. The apparent activation energy (E_a) changes with respect to both NO and O_2 concentration (see Table 2).

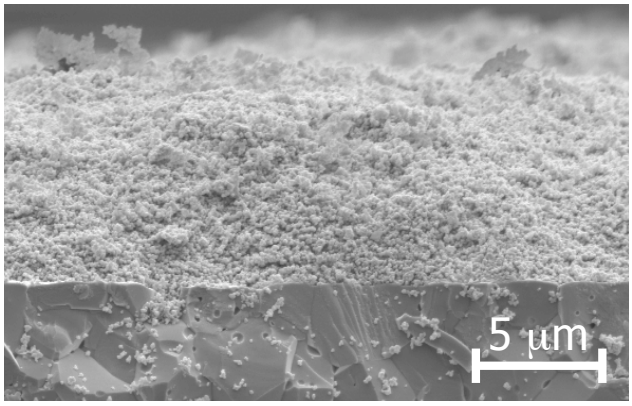

(a)

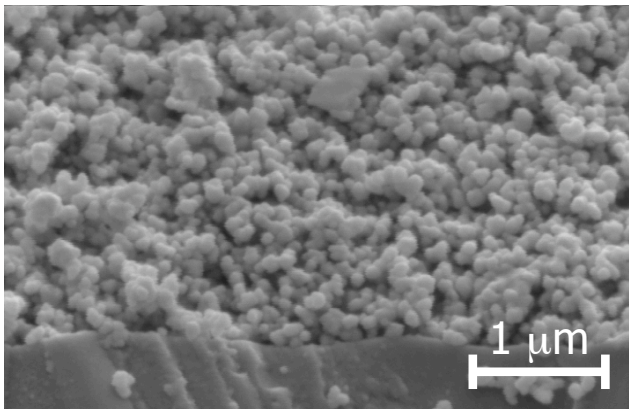

(b)

Figure 1:

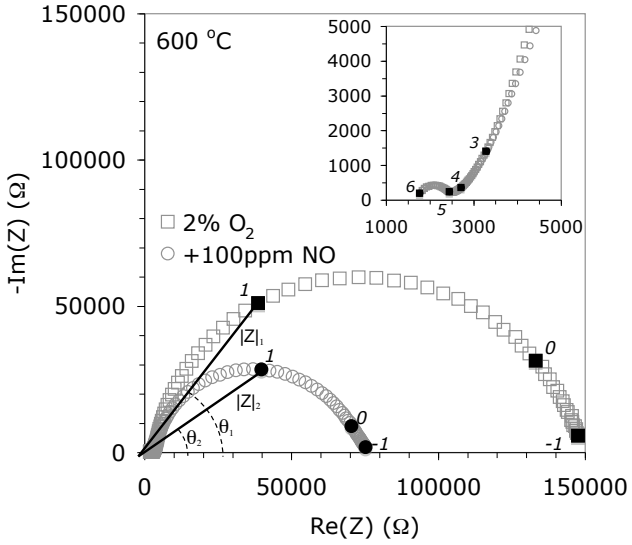
600 °C
2% O2
+100ppm NO
-Im(Z) (Ω)
Re(Z) (Ω)
150000
100000
50000
0
0
50000
100000
150000
5000
4000
3000
2000
1000
0
1000
3000
5000
1
0
-1
3
4
5
6
|Z|1
|Z|2
θ1
θ2

Figure 2:

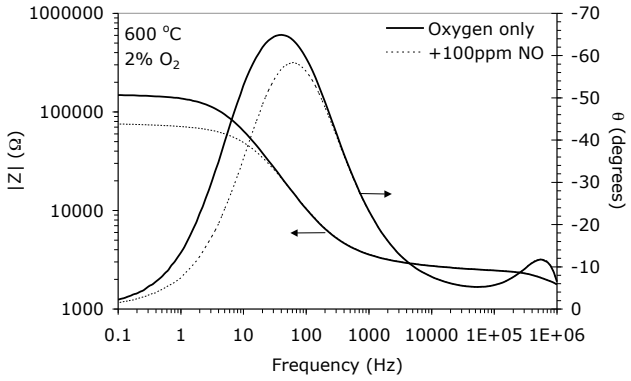
1000000
100000
10000
1000
|Z| (Ω)
600 °C
2% O2
Oxygen only
+100ppm NO
-70
-60
-50
-40
-30
-20
-10
0
θ (degrees)
0.1
1
10
100
1000
10000
1E+05
1E+06
Frequency (Hz)

(a)

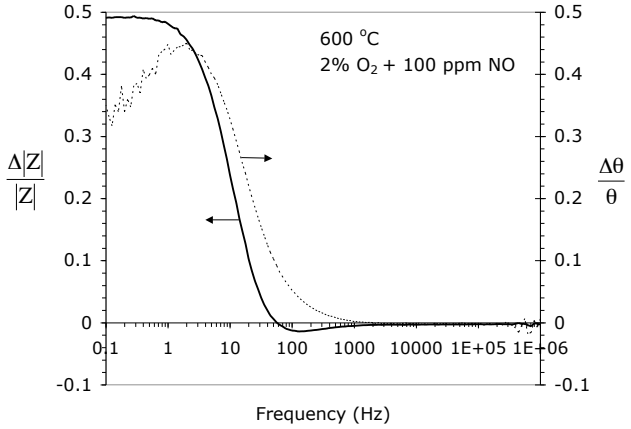
0.5
0.4
0.3
0.2
0.1
0
-0.1
Δ|Z| / |Z|
600 °C
2% O2 + 100 ppm NO
Δθ / θ
0.1
1
10
100
1000
10000
1E+05
1E+06
Frequency (Hz)

(b)

Figure 3:

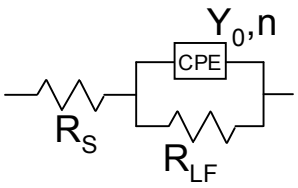

Figure 4:

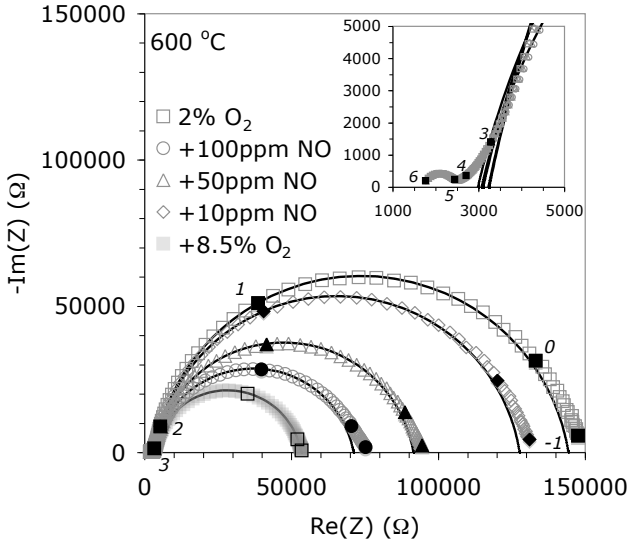
600 °C
2% O2
+100ppm NO
+50ppm NO
+10ppm NO
+8.5% O2
-Im(Z) (Ω)
Re(Z) (Ω)
150000
100000
50000
0
0
50000
100000
150000
5000
4000
3000
2000
1000
0
1000
3000
5000
1
2
3
4
5
6
0
-1

Figure 5:

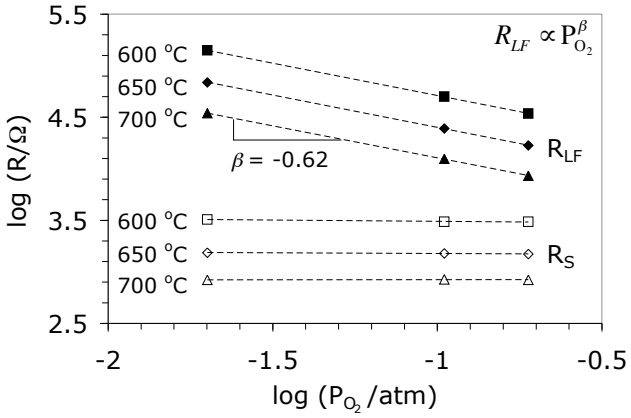
$R_{LF} \propto P_{O_2}^{\beta}$
600 °C
650 °C
700 °C
β = -0.62
R_{LF}
600 °C
650 °C
700 °C
R_S
log (R/Ω)
log (P_{O_2}/atm)

(a)

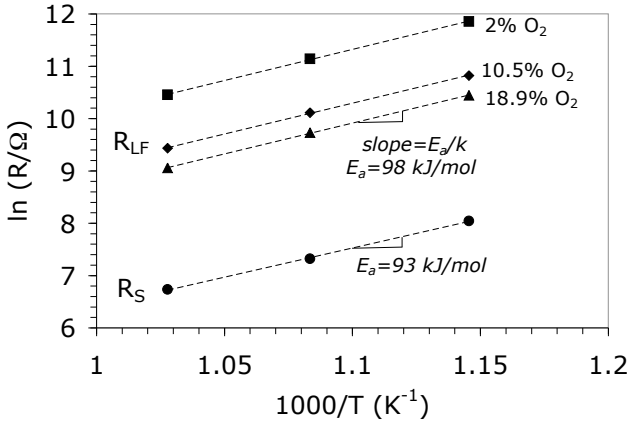
2% O_2
10.5% O_2
18.9% O_2
R_{LF}
slope=E_a/k
E_a=98 kJ/mol
R_S
E_a=93 kJ/mol
ln (R/Ω)
1000/T (K^{-1})

(b)

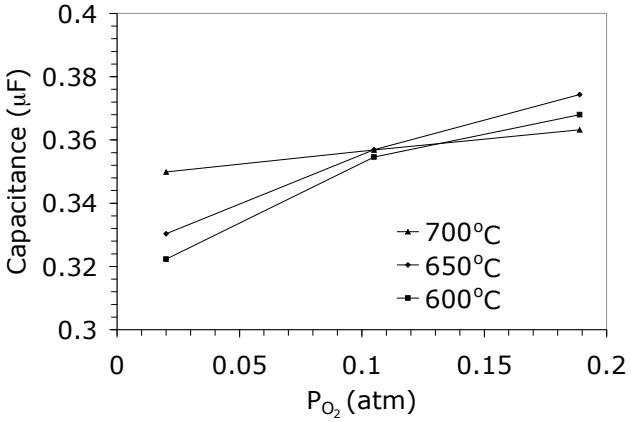
700°C
650°C
600°C
Capacitance (μF)
P_{O_2} (atm)

(c)

Figure 6:

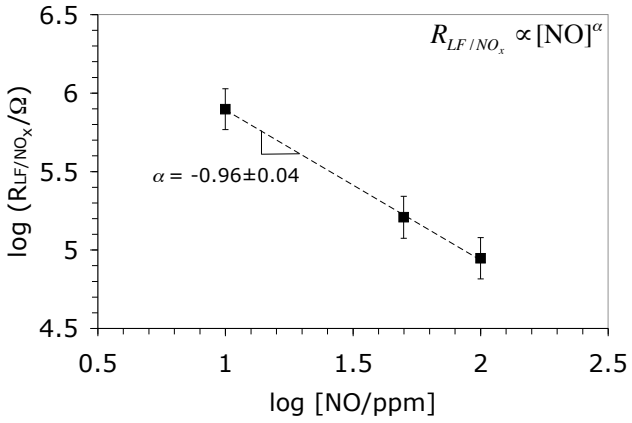
$R_{LF/NO_x} \propto [NO]^{\alpha}$
α = -0.96±0.04
log (R_{LF/NO_X}/Ω)
log [NO/ppm]
6.5
6
5.5
5
4.5
0.5
1
1.5
2
2.5

(a)

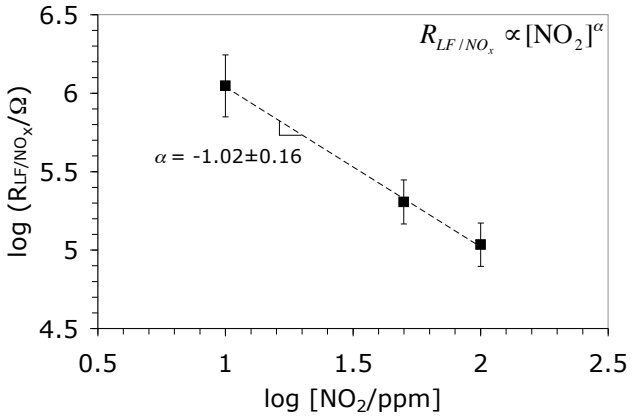
$R_{LF/NO_x} \propto [NO_2]^{\alpha}$
α = -1.02±0.16
log (R_{LF/NO_X}/Ω)
log [NO_2/ppm]
6.5
6
5.5
5
4.5
0.5
1
1.5
2
2.5

(b)

Figure 7:

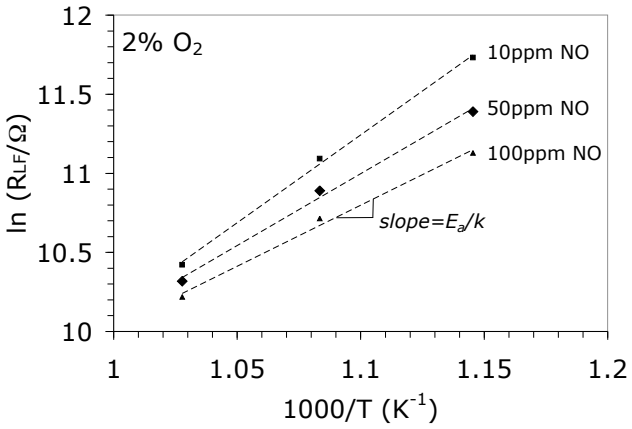
12
11.5
11
10.5
10
2% O2
10ppm NO
50ppm NO
100ppm NO
slope=Ea/k
ln (RLF/Ω)
1
1.05
1.1
1.15
1.2
1000/T (K-1)

Figure 8: